Desalination 556 (2023) 116541

Contents lists available at ScienceDirect

Desalination

journal homepage: www.elsevier.com/locate/desal

Current distribution along electrodialysis stacks and its influence on the current-voltage curve: behaviour from near-zero current to limiting plateau

Antonia Filingeri [a], Luigi Gurreri [b,*], Michele Ciofalo [a], Andrea Cipollina [a,*], Alessandro Tamburini [a], Giorgio Micale [a]

[a] Dipartimento di Ingegneria, Università degli Studi di Palermo, viale delle Scienze ed. 6, 90128 Palermo, Italy
[b] Dipartimento di Ingegneria Elettrica, Elettronica e Informatica, Università di Catania, viale Andrea Doria 6 ed. 3, 95125 Catania, Italy

HIGHLIGHTS

- An ED stack with 40 cm path length, provided with 4-segment electrodes, was tested.
- The CVCs were recorded for brackish water and final stage seawater desalination.
- At the limiting voltage, V_{lim}, ~50 % of current (I) flowed through the first segment.
- At V_{lim} the relative standard deviation of the I distribution was ~40 % to 70 %.
- The nexus between I maldistribution and desalination performance drop was stressed.

GRAPHICAL ABSTRACT

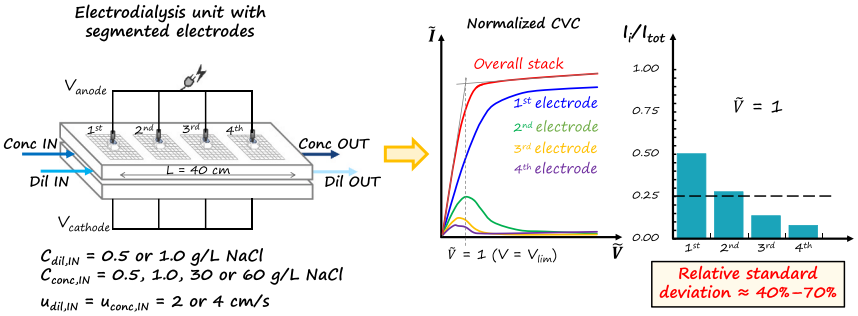

ARTICLE INFO

Keywords:
Electrode segmentation
Current profile
Concentration distribution
Brackish water
Seawater

ABSTRACT

The current maldistribution along the flow path of electrodialysis (ED) units is a well-known phenomenon. However, it has been poorly quantified via experimental tests so far. This work aimed at measuring the current distribution in an ED stack with 40 cm path length, provided with four-segment electrodes. The current-voltage curve (CVC) of each segment was recorded under several operating conditions of inlet concentrations and feed velocity. In the CVC of the first segment, the current increased approaching a saturation, while in that of the remaining segments it passed through a maximum and then settled at near-zero values when high voltage values were applied. The current fraction on the segments decreased from inlet to outlet. In the overall CVC's first region, up to ~50 % of total current flowed through the first quarter of stack. As the voltage increased, the current fraction increased in the first segment, while it decreased in the other ones tending to vanish. At the limiting condition, the relative standard deviation of the current fraction distribution ranged from 40 % to 68 %. This strong non-uniformity in the ED stack, which may represent one stage of an industrial plant, implies that the design of commercial units must be improved.

Abbreviations: CVC, Current-voltage curve; ED, Electrodialysis; IEM, Ion-exchange membrane; LCD, Limiting current density.

* Corresponding authors.
E-mail addresses: luigi.gurreri@unict.it (L. Gurreri), andrea.cipollina@unipa.it (A. Cipollina).

https://doi.org/10.1016/j.desal.2023.116541
Received 15 December 2022; Received in revised form 21 February 2023; Accepted 28 February 2023
Available online 27 March 2023

1. Introduction

Electrodialysis (ED) [1] is a well-established electro-membrane process, recently proposed for emerging applications in several fields as pharmaceutical industry, food processing, and biotechnology, as well as wastewater treatment [2,3]. However, the main application of ED at commercial scale is brackish water desalination to produce drinking water [4]. In this field, ED is competitive with the leading desalination technology represented by Reverse Osmosis (RO), and covers ~2 % of the global desalination capacity [5]. Recently, ED and ED-derived processes have gained attention also for the development of hybrid schemes to reduce energy consumption, valorize brine, increase water production and remineralize the RO permeate [6–10]. These combinations exhibited interesting results, but conceal the current inadequacy of standalone ED systems for seawater desalination. Indeed, techno-economical limitations characterize ED processes of high-salinity solutions (like seawater) aimed at producing low-salinity products (like drinking water). Attaining a good trade-off between productivity and specific energy consumption, which are the two most representative performance metrics, has been unfeasible so far. In recent years, considerable efforts have been devoted to modelling [11–13] and experimental [14–17] studies of seawater desalination via ED, highlighting these process limitations. It follows that ED is not yet competitive compared to conventional desalination technologies [4,18], unless dilute solutions are treated.

An important bottleneck of ED systems is the limiting current density (LCD), which can be experimentally determined from the current-voltage curve (CVC). Electro-membrane systems are characterized by CVCs that usually exhibit three different regions [19–21], as reported in Fig. 1: in the first region, which is mainly Ohmic, the current increases approximatively linearly with voltage; in the second (or limiting) region, the rate of current increase with voltage is reduced and may even tend to zero (saturation), meaning that a severe increase of apparent resistance occurs; in the over-limiting region, other phenomena of ion transport (as water splitting and/or electroconvection) arise, sustaining current values higher than the limiting one. The limiting current can be determined from the intersection point between the linear trend at low current and the tangent line to the second region [22]. The corresponding LCD (limiting current over active membrane area ratio) is taken as a reference threshold in ED practice to avoid the risks of fouling, scaling, and membrane deterioration due to extreme pH values that may arise in overlimiting conditions.

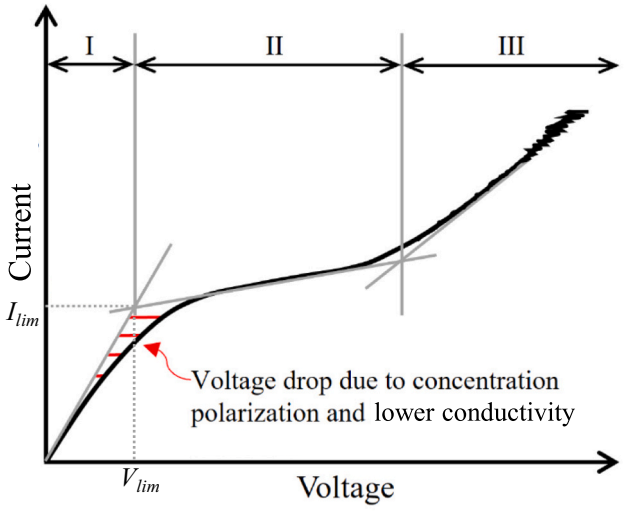

Fig. 1. Typical CVC curve with three distinct regions characterizing ED apparatuses. The graphical identification of limiting current and limiting voltage is reported. Adapted from [1].

The CVC saturation and the occurrence of LCD is usually ascribed to concentration polarization phenomena [23] (concentration gradient developed in the boundary layer adjacent to the IEM surface). The difference in ions mobility between the solution and the membrane results in a concentration depletion in the diluate compartment and a concentration enrichment in the concentrate compartment [24]. The diffusional limiting current density is theoretically associated with the local occurrence of a null concentration at the diluate-membrane interface [25–27]. However, beyond the general features that are shared by the CVCs of different electro-membrane systems, a clear distinction must be made to differentiate apparatuses commonly used for the characterization of ion-exchange membrane (IEM) from commercial ED stacks. In the former case, compact cells with two [28–31] or more (e.g., six [21,32]) compartments are used to build the characteristic CVC of the membrane without producing any desalination effect, thus producing a proper polarization curve. In the latter case, the application of voltage results in the desired effect of desalination of the diluate compartment. This concentration depletion in the longitudinal direction causes a decrease of the average concentration and thus an increase of the average electrical resistance. Moreover, the average concentration is lower than the mean value between its inlet and outlet values. Indeed, resistance and current are related by a mutual dependence by means of the diluate concentration. As a result, all these quantities are non-linearly distributed along the fluid flow path, which is characterized by denser current lines close to the inlet region [33], where a larger portion of desalination occurs. The phenomenology involved is even more complex if one considers that, according to the micro-heterogeneous model, the IEMs resistance depends on the diluate concentration [34,35]. All of the above phenomena contribute to the departure from the initial proportionality and to the existence of an LCD in the CVC of ED processes. Interestingly, from a simple mass balance, it can be observed that the in-out concentration difference increases as the electric current increases and as the flow rate decreases, thus showing similar (at least qualitatively) features compared to concentration polarization [1]. Despite all this, the influence of desalination effects along the flow path on the CVC is ignored in most of the literature on ED, while only concentration polarization is typically mentioned [36–39].

Beyond the influence on the LCD, the longitudinal distributions within ED stacks underlie other critical issues. By fixing the concentration target, the detrimental influence of the longitudinal distributions on the process performance is twofold. On one hand, the resistance's distribution makes its average value increase, thus causing an increase of Specific Energy Consumption (SEC). On the other hand, the sharp onset of a high concentration gradient between diluate and concentrate channels increases the average driving force for unwanted transport phenomena (salt diffusion, osmosis, and electro-osmosis), thus reducing the current efficiency. This, in turn, determines the requirement of a higher electric current to achieve the diluate concentration target, thus further increasing the SEC.

In contrast, an ED process with multiple electrical stages can work with more even distributions, benefiting of a higher current efficiency and of a lower SEC. For example, in [12] a process model predicted a reduction of SEC from 4.6 kWh/m^3 to 1.9 kWh/m^3 for seawater desalination by switching from a fixed voltage configuration to a fixed current (i.e., equal average current for all stages) configuration in a four-stage system with 43 cm path length per stage. In addition, multiple stages can be designed with a different number of cell pairs or with different membrane types to further enhance the process [16,17,40]. Multi-stage configurations and other systems with electrode segmentation were investigated in ED [11,12,14,16,17,40–42], as well as in other electro-membrane processes as reverse electrodialysis (RED) [43–47], ED with bipolar membranes [48], electrochemical fuel cells [49,50], and redox flow batteries [51,52]. Several studies showed that multi-staging is a strategy that offers interesting solutions to ensure that the ED stacks can work more efficiently. However, the issues of current distribution

and consequent performance fall remain at least partially unsolved in industrial plants, where each single stage may have a path length in the order of 1 m [36,53–56]. Analogous issues arise in batch ED operation [57], where (i) the spatial variable is substituted by time and (ii) dynamic voltage operations can act in the direction of performance improvement [58,59]. However, batch operations are not recommended for industrial applications.

The distribution of current and concentration in ED units has been known since the past century. In 1968, Sonin and Probstein [60] developed a hydrodynamic-based theory of ED. The distribution of current, electric field and salt concentration were studied via analytical and numerical solutions for either uniform or parabolic velocity profiles in ED stacks with spacerless channels and ideal membranes, by distinguishing two scenarios of either high or low concentration polarization. The results provided an interesting description of the distribution phenomena, as well as of the current-voltage curve. However, the agreement with the available experimental results was only qualitative. In 1972, Grossman and Sonin [61] used an ED stack with unobstructed compartments and with electrodes segmented into fifteen elements, finding a fair agreement with the previous theoretical results on current profiles decreasing from inlet to outlet. In experiments with seawater, Tanaka found a decreasing current distribution that could be approximated by a quadratic expression [62]. He assumed the same law in several modelling studies of continuous [63,64] and batch [65] ED systems. The current distribution became more inhomogeneous as the applied voltage (or the average current density) increased and the diluate inlet concentration decreased [63,64]. Ghorbani and Ghassemi [66] experimentally observed a nonlinear concentration profile along both concentrate and diluate compartments in a lab-scale ED stack, showing that most desalination was compressed in the first portion of the path length. However, they did not measure the current profile.

Concentration and current profiles can develop with different shapes, depending on the operating conditions. Tanaka [67] performed experiments for seawater concentration with linear velocities of 0.5 cm/s and 5 cm/s for the concentrate and diluate compartments, respectively, and with closed-loop concentrate. He found that the current decreased little along the stack, probably because the resistance increase in the diluate was partially compensated by the resistance reduction in the concentrate. By feeding a segmented-electrode ED stack with seawater in counter-flow mode and with asymmetric velocity (~6–7 higher in the diluate compartments), Mitko and Turek [68] measured the current profiles, finding the maximum somewhere in the middle, and estimated sigmoidal shaped concentration profiles in the concentrate channel. The same authors measured similar current profiles also in another work, claiming that the reasons behind their shape were unclear [69].

Thus, although the longitudinal distribution of electric current in ED stacks is a phenomenon, known in academia and industry, that affects the process performance, only qualitative or fragmentary data are available. Even the easy access to this parameter by modelling tools has been almost ignored [1,70] apart from rare exceptions [12,63,64]. The aim of this work is to provide a first breakthrough towards a more complete experimental quantification and analysis of the current distribution. By using an ED experimental setup equipped with segmented electrodes, CVCs of each stack segment were recorded and analyzed across the first and the second region of the overall CVC. The distribution of electric current and its mutual relation with that of the salt concentration in the diluate channel was discussed, showing that severe problems of maldistribution take place even in a stack with a relatively short path length (40 cm). The experiments were carried out with different values of inlet concentration and fluid velocity, mimicking either brackish water or last-stage seawater desalination processes, thus providing useful information in a broad spectrum of operating conditions.

2. Experimental setup and procedure

ED tests were conducted in continuous mode to obtain Current Voltage Curves (CVCs) adopting a stack equipped with four couples of segmented electrodes. CVCs were obtained for each electrode pair by voltammetry experiments carried out under different operating conditions of inlet concentration (mimicking either brackish water or seawater) and velocity. The first (often referred to as “Ohmic”) and the second (also known as “limiting”) region of the overall CVC were characterized. For each step of applied voltage, the outlet conductivities were also measured. Current efficiency and concentration profiles were calculated, from the experimental information.

2.1. Materials and setup

ED stack (REDstack B.V., The Netherlands) was provided with segmented electrodes, and consisted of ten cell pairs and four electrode couples. The membrane active area was 10 cm (width) × 40 cm (length), while the active area of each electrode segment was 10 × 10 cm^2. Fujifilm CEMs and AEMs Type-10 (Fujifilm Manufacturing Europe B.V., The Netherlands) and titanium and iridium-MMO (mixed metal oxide) coated electrodes (Magneto Special Anodes B.V., The Netherlands) were used. Woven spacers with a thickness of 155 μm were interposed between the membranes to form both concentrate and diluate compartments [71,72]. The main membrane properties, provided by the manufacturer, are reported in Table 1.

Synthetic salt solutions were prepared from demineralized water and NaCl (>99.5 % purity, Saline di Volterra s.r.l., Italy). The inlet concentration couples values were fixed to represent the desalination of brackish water and the final stages of a seawater desalination system. The tests were performed in single-pass mode for both solutions, which crossed the stack in co-flow arrangement with velocities of either ~2 or 4 cm/s. The operating conditions for inlet concentration and fluid velocity are reported in Table 2. All the experiments were carried out at room temperature (~20 °C).

The electrode rinse solution (ERS) was an aqueous solution with 0.3 mol/L $K_3Fe(CN)_6$ (≥99 % purity, Honeywell Fluka™, China), 0.3 $K_4Fe(CN)_6{\cdot}3H_2O$ (≥99 % purity, Honeywell Fluka™, China), and 0.25 NaCl (>99.5 % purity, Saline di Volterra s.r.l., Italy). The ERS flowed through one electrode compartment (from its first segment towards the fourth one) and then through the other compartment (from its first segment towards the fourth one). Fig. 2 shows a schematic representation of the experimental setup.

All the solutions were pumped through the stack by magnetic gear pumps (Fluid-o-Tech FG204). Pressure gauges (Cewal) were installed downstream of the inlet tanks. A calibration curve was built to set the operating conditions of fluid velocity. During each test, the flow rate was checked as the volume of fluid from the stack collected in a graduated cylinder over the time. A portable conductivity-meter (WTW 314i) was used to measure the electric conductivity of inlet and outlet solutions of concentrate and diluate. Each electrode couple was connected to a different power supply (Elektro-Automatik EA-PS 2042-10 B) and a multimeter (Fluke 175) measuring the electric current.

2.2. Experimental procedure

Before starting the ED experimental campaign, external and internal leakage tests were carried out to ensure that leakages were negligible [73].

The starting point to build the CVCs was an applied current equal to zero. This allowed measurement of open circuit voltage (OCV) value, at each electrode pair, in the experiments with a salinity gradient between the feed solutions. Then, staircase voltammetry was applied by increasing steps of applied voltage, fixed equal for the four electrode couples, each lasting at least eight-to-ten times the residence time of the solutions in the stack, thus ensuring the attainment of steady conditions.

Table 1
Properties of the Fujifilm Type 10 ion-exchange membranes used in this study.

	Thickness (dry) [μm]	Areal resistance[a] [Ω cm^2]	Permselectivity[b] [%]	IEC [meq/g]	Water permeability [mL/(m^2 h bar)]	Burst strength [kg/cm^2]
AEM	125	1.7	95	1.8	6.5	2.8
CEM	135	2.0	99	1.5	6.5	2.8

[a] Measured in 2 mol/L NaCl solution.
[b] Evaluated from measurements of membrane potential with 0.05 mol/L and 0.5 mol/L KCl solutions.

Table 2
Operating conditions for fluid velocity and inlet concentration of the salt solutions.

	Concentrate	Diluate
Inlet concentration [g/L NaCl]	0.5	0.5
	30	
	1	1
	30	
	60	
Fluid velocity [cm/s]	2	
	4	

In order to investigate the distribution of current along the stack at both under-limiting and limiting conditions, the applied voltage was increased up to attaining a full plateau of the total electric current. The steady-state values of electric current for each electrodes couple were recorded to build the overall CVC. The latter was represented as the overall current density averaged over the four electrode segments (total current divided by the total area) as a function of the applied voltage.

For any operating condition (inlet concentrations and velocity), the Isaacson and Sonin graphical method (two tangent lines) [22] was used in the overall CVC to identify the two regions and the limiting current density (LCD) of the stack. The values of LCD were compared with those of the current density recorded at the maximum current efficiency, which provides a useful reference as a "practical" threshold value of current [74]. The current efficiency, η, was calculated as:

$$\eta = \frac{z\,F\left(Q_{dil,IN}C_{dil,IN} - Q_{dil,OUT}C_{dil,OUT}\right)}{N_{CP}I\,M_w} \tag{1}$$

where Q_{dil} (L/s) and C_{dil} (g/L) are the total flowrate and the salt concentration in the diluate compartment, respectively, N_{CP} is the cell pairs number, I (A) is the total electric current, M_w (g/mol) is the NaCl molecular weight, z is the ion valence (1) and F (C/mol) is the Faraday constant; the sub-scripts *IN* and *OUT* refer to the stack inlet and outlet, respectively. The conductivity of the inlet solutions was measured before starting the test, while the conductivity of the outlet solutions was measured at the steady state attained at each applied voltage. The corresponding salt concentrations were calculated by an empirical correlation [75].

In order to draw general considerations from the CVC of each electrode segment, values of applied voltage and measured current were normalized as follows. The reference values for current and voltage were the limiting current, I_{lim}, and the "limiting voltage", V_{lim}, respectively, of the stack. They were identified from the overall CVC as the coordinates of the intersection point of the two tangent lines (see Fig. 1). In other words, the limiting voltage is defined as the boundary value between the first and the second region of the overall CVC, and can be considered a "safe" operational value providing high currents [42]. Normalized values of current at the i-th electrode segment, $\widetilde{I}_i$, were calculated as:

$$\widetilde{I}_i = \frac{I_i}{I_{lim}} \tag{2}$$

where I_i is the current measured at the i-th electrode segment. Likewise, the total current is normalized as I_{tot}/I_{lim}, Normalized values of voltage were calculated as:

$$\widetilde{V} = \frac{V - OCV}{V_{lim} - OCV} \tag{3}$$

where V is the applied voltage (equal for all electrode segments) and

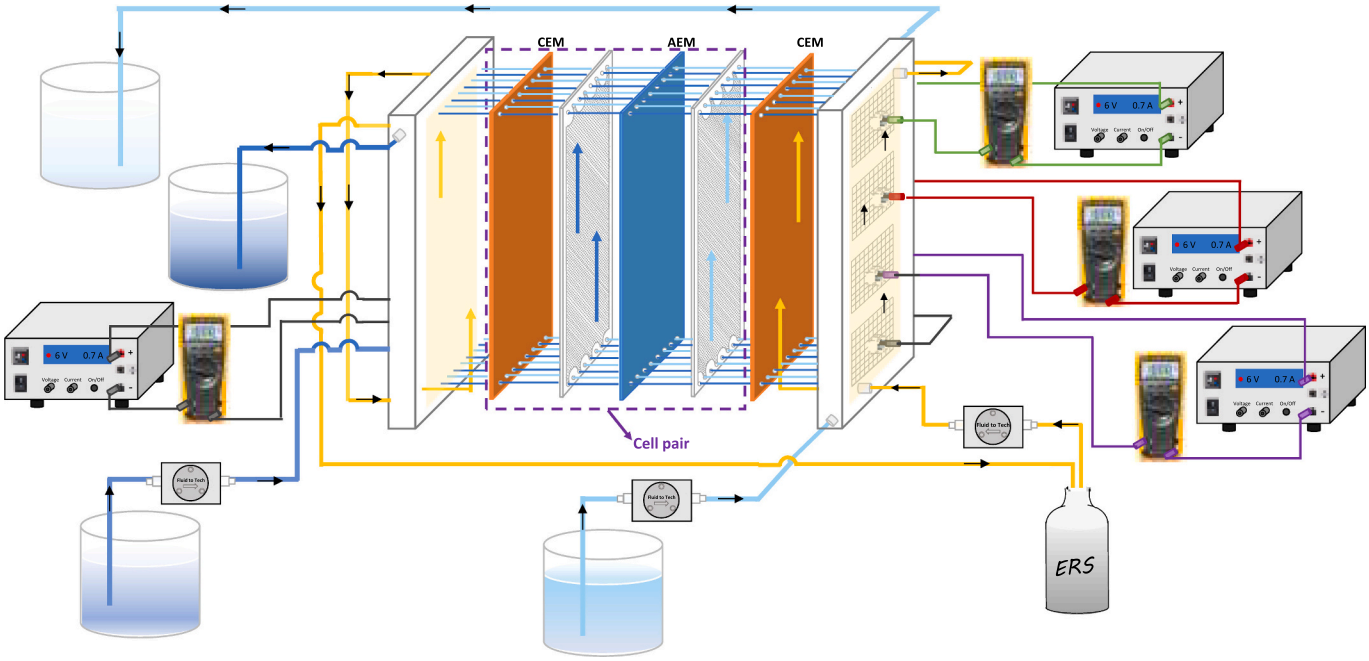

Fig. 2. Schematics of the ED set-up with some auxiliaries.

OCV is the average open circuit voltage recorded at the four-segment electrodes.

2.3. Estimation of concentration profile in the diluate compartment

The distribution of the salt concentration along the diluate compartment is a crucial feature together with the distribution of electric current to provide a more complete characterization of the stack behaviour. However, the concentration profile along the flow path is not directly accessible via a conventional ED setup such as the one used in the present study. To overcome this limitation, the collected experimental data were used to estimate the concentration values. From a mass balance, by assuming that the current efficiency was uniform along the stack and equal to that calculated with Eq. (1), and by knowing the measured electric current at each electrode couple, the diluate outlet concentration from the first three segments was estimated as follows:

$$C_{dil,OUT,i} = C_{dil,IN,i} - \eta \frac{N_{CP} I_i M_w}{z F Q_{dil,AVE}} \quad (4)$$

where $Q_{dil,\,AVE}$ refers to the average (stack inlet-outlet) diluate flow rate, and the subscript i refers to the i-th segment (i.e., 1, 2, or 3). $C_{dil,IN,1}$ is simply the concentration of the diluate feed; thus, Eq. (4) was first solved for the first segment. The calculated value of $C_{dil,OUT,1}$ was then used as inlet concentration to second segment ($C_{dil,IN,2}$) to calculate $C_{dil,OUT,2}$, and so on. $C_{dil,OUT,4}$ was obtained from the conductivity of the diluate product. Current and concentration profiles in the segments were represented in the form of current fraction (with respect to the total four-segment current) and diluate concentration normalized by the diluate feed concentration.

2.4. Uncertainty analysis

For variables directly measured such as current and voltage, the individual uncertainties were estimated by considering the instruments accuracy reported in their technical specifications. More in detail, the conductivity-meter WTW 314i has an accuracy of ±(0.5 % +1 digit), while the multimeter Fluke 175 has an accuracy of ±(1 % +3 digit) and ±(0.15 % +2 digit) for current and voltage, respectively. The uncertainty in the flow rate measurements was estimated by considering (i) the accuracy of the cylinder used to collect the fluid and (ii) an operator error of 0.5 s on a total measurement time of 60 s. The uncertainty about the membrane area was neglected. In all these cases, the uncertainty was not graphically relevant, so that error bars were not included in the graphs. On the other side, the error propagation theory [76] was implemented to calculate the experimental error for estimated variables, i.e., current efficiency, current fraction and diluate concentration inside the stack, for which errors were found to be small, yet visible. Therefore, graphs reporting these quantities were provided with error bars.

Several tests were carried out in duplicate, showing a good repeatability with a percentage deviation lower than 4 % for the measured values of current and of (diluate and concentrate) outlet conductivities.

3. Results and discussion

The first part of this section will focus on the study of the CVC and desalination performance (diluate outlet concentration and current efficiency) of the stack (Section 3.1). Next, the single CVCs of each electrode couple will be analyzed (Section 3.2). Then, the longitudinal distribution of current and the estimated profiles of diluate concentration will be presented (Section 3.3). The selected results refer to tests performed at speeds of either 2 cm/s or 4 cm/s and feedwater concentrations of either $C_{dil,IN} = C_{conc,IN} = 1$ g/L or $C_{dil,IN} = 0.5$ g/L, $C_{conc,IN} = 30$ g/L. Results obtained with other operating conditions are reported in detail in the Supplementary data. However, an overall, albeit summarized, comparison of all tests will be reported and discussed in Section 3.4.

3.1. Overall CVC and performance of the stack

3.1.1. Feed concentrations 1–1 g/L

Overall results characterizing the stack for tests performed at an inlet concentration of 1 g/L for both diluate and concentrate and at velocities of either 2 cm/s or 4 cm/s for both streams are reported in Fig. 3. The CVCs (Fig. 3a) started from the origin of the axes, as the open circuit voltage (OCV) was zero. The first region, often named Ohmic region, was approximatively linear. The areal stack resistance (reciprocal of the CVC curve slope) at low current density was ~0.095 Ω m^2 and 0.090 Ω m^2 for the test at 2 cm/s and 4 cm/s, respectively. The second region of the CVC, referred to as plateau or limiting region, was characterized by a significant reduction of the slope, i.e., a gradual rise of the apparent resistance, until attaining an almost horizontal asymptote of the current.

In a more detailed analysis, the characteristics of both regions of the CVC of an ED stack are typically ascribed to both Ohmic and non-Ohmic effects. On one hand, as the voltage increases the current increases, thus reducing via desalination the average concentration of the diluate, which results in a higher resistance. It can even be argued that this resistance associated to a "longitudinal polarization" is not properly Ohmic, as it is not constant. Indeed, in the reverse electrodialysis jargon the voltage drop (reduction of electromotive force) due to the axial variation of the concentrations and the resistance associated to it are usually indicated as "non-Ohmic" [77,78]. On the other hand, at higher currents, concentration polarization becomes more pronounced, thus causing a further increase of the (non-Ohmic) resistance. This is particularly relevant at very low concentrations in the diluate channel, which can lead to a dramatic depletion of ions across the membrane-solution boundary layer. In conventional measurements reported in the literature to determine the incurrence of LCD, as well as in the following results reported in the section, it is hard to identify the influence of the two phenomena, due to the lack of information on the current distribution. However, measuring current distribution using segmented electrodes stack can provide an interesting insight on the actual influence of the current distribution in the determination of LCD conditions, as presented in the Sections 3.2 and 3.3.

The phenomena causing an increase in the electrical resistance are small at low current densities; therefore, the CVC started linearly at $i \rightarrow 0$. At higher applied voltages, however, they become non-negligible, so that a loss of linearity can be observed in the final part of the first region. As the voltage is further increased, the stack resistance increases more and more, producing in the CVC (i) the "knee" that covers the initial part of the second region and (ii) the plateau. Regarding the effect of the velocity, higher values led to a longer and little more sloped (on average) first region of the CVC. A dramatic influence was observed in the limiting region. The LCD obtained via the Isaacson and Sonin method [22] was roughly doubled (from 10.6 A/m^2 to 22.6 A/m^2) when the velocity was doubled from 2 cm/s to 4 cm/s.

For the two values of velocity, Fig. 3b reports the diluate outlet concentration as a function of the applied voltage. In each $C_{dil,OUT}$ .V curve, two "regions" with different features can be clearly distinguished, reflecting the i-V behaviour. In the first region, the concentration decreased linearly with the applied voltage due to the corresponding almost linear increase in current. The second region exhibited a plateau, by attaining minimum values (~0.10 g/L and 0.15 g/L for tests at 4 cm/s and 2 cm/s, respectively) associated with the practically null increase in current (see Fig. 3a). Therefore, operating ED processes in this region would not be economically profitable as the energy consumption would increase without achieving any desalination benefit.

The diluate concentration can be regarded as a combined result of current density (Fig. 3a) and current efficiency (Fig. 3c). In both cases of fluid velocity tested, η increased from a minimum of ~85 % at low applied voltage to a maximum of ~95 %, and remained steady or decreased slightly in the range of voltage of the CVC's second region.

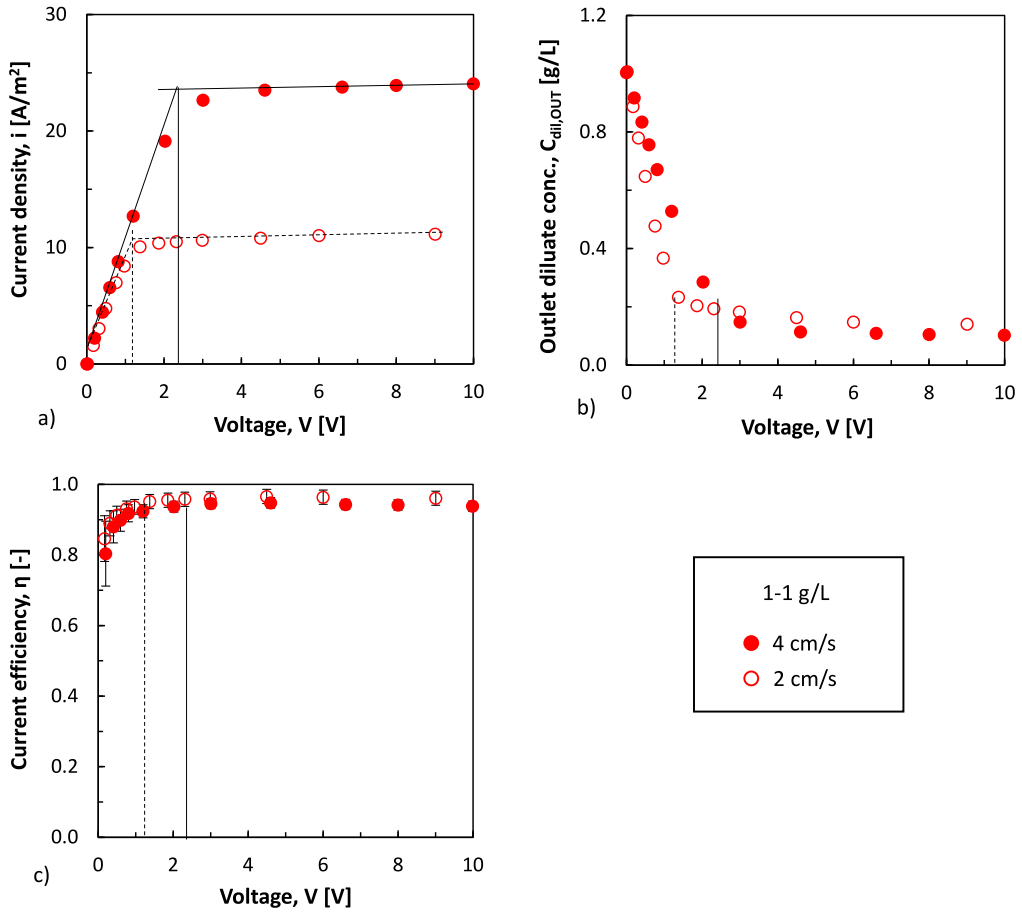

Fig. 3. a) Current density, b) diluate outlet concentration and c) current efficiency as functions of the applied voltage for tests performed at inlet concentrations of $C_{dil,IN} = C_{conc,IN} = 1$ g/L and velocities of both solutions of either 2 or 4 cm/s. Dashed and continuous vertical lines identify the boundary between the first and the second region at 2 and 4 cm/s, respectively.

Despite our data at low voltages were affected by larger error bars, the increase of the current efficiency exhibiting a maximum as a function of voltage (or current) in the first region of the CVC confirms the results observed in several experiments [74,79,80]. This behaviour is a complex outcome from a balance of electro-migration against unwanted transport mechanisms of co-ions (back-diffusion) and water (osmosis/electro-osmosis), which are driven by direct and indirect effects of the increasing current itself and are not uniform along the flow path [79]. The values of current density at which the current efficiency was the highest were 23.5 A/m^2 and 10.6 A/m^2 at 4 cm/s and 2 cm/s, respectively, which were very close to the values of LCDs identified graphically from the CVCs [74].

3.1.2. *Feed concentrations 0.5–30 g/L*

Similar features, but also some marked differences, were observed in the tests with a high salinity gradient between the feed streams. For example, Fig. 4 reports the same charts as Fig. 3 but for the tests performed with inlet concentrations $C_{dil,IN} = 0.5$ g/L and $C_{conc,IN} = 30$ g/L. An average OCV over the four electrode segments of ~1.80 V and ~1.74 V was measured at 4 cm/s and 2 cm/s, respectively. The lower value of OCV at the lower value of velocity was due to the larger osmosis and salt back-diffusion (higher residence time). The stack resistances at $i \rightarrow 0$ were ~ 0.096 Ω m^2 and 0.073 Ω m^2 for 4 cm/s and 2 cm/s, respectively. The first part of the CVC was approximately linear and covered a normalized voltage $\widetilde{V}$ up to ~50 %. The fluid velocity had again a more significant effect on the limiting behaviour. The LCD values were 12.4 A/m^2 and 6.6 A/m^2 at 4 cm/s and 2 cm/s, respectively. They are significantly lower than those observed at equal inlet concentrations of 1 g/L (Fig. 3).

Fig. 4b also shows that the diluate outlet concentration is higher than the inlet one at low applied voltage and thus low current. This indicates that unwanted transport phenomena of salt diffusion, osmosis and electro-osmosis prevail on the electro-migration of salt ions. Therefore, the current efficiency is even negative. As the current increases, a "critical" condition occurs, in which the contrasting effects are perfectly balanced, so that the outlet concentration is equal to the inlet one. The current density providing this condition was referred to as "critical current density" (CCD) [74]. For the present tests, the CCD was ~2.1–2.2 A/m^2, being less affected by the fluid velocity. At current densities higher than the CCD, a desalination effect is obtained.

Fig. 4c shows that η increased in the first region due to the rising predominance of electro-migration over unwanted transport phenomena up to attaining maximum values of 84 % and 76 % at velocities of 4 cm/s and 2 cm/s, respectively. Also in these tests, the current densities (12.5 A/m^2 at 4 cm/s, 6.1 A/m^2 at 2 cm/s) providing the highest η were practically coincident with the LCDs. As the applied voltage increased in the plateau region, η slowly decreased, as already observed in previous experiments [74,79].

Experimental data collected with different inlet concentrations couples are reported in the Supplementary data (Figs. S1–S3). Overall, very similar qualitative results were found compared to those reported and discussed above in the main text. LCDs varied in the range of ~5.5–27.3 A/m^2 depending on the inlet diluate concentration and solution velocity. The outlet concentration of the diluate compartment in the plateau region was of ~0.1–0.15 g/L for tests at $C_{dil,IN} = 1$ g/L and $C_{conc,IN} = 30$ or 60 g/L while the minimum in $C_{dil,OUT}$ equal to

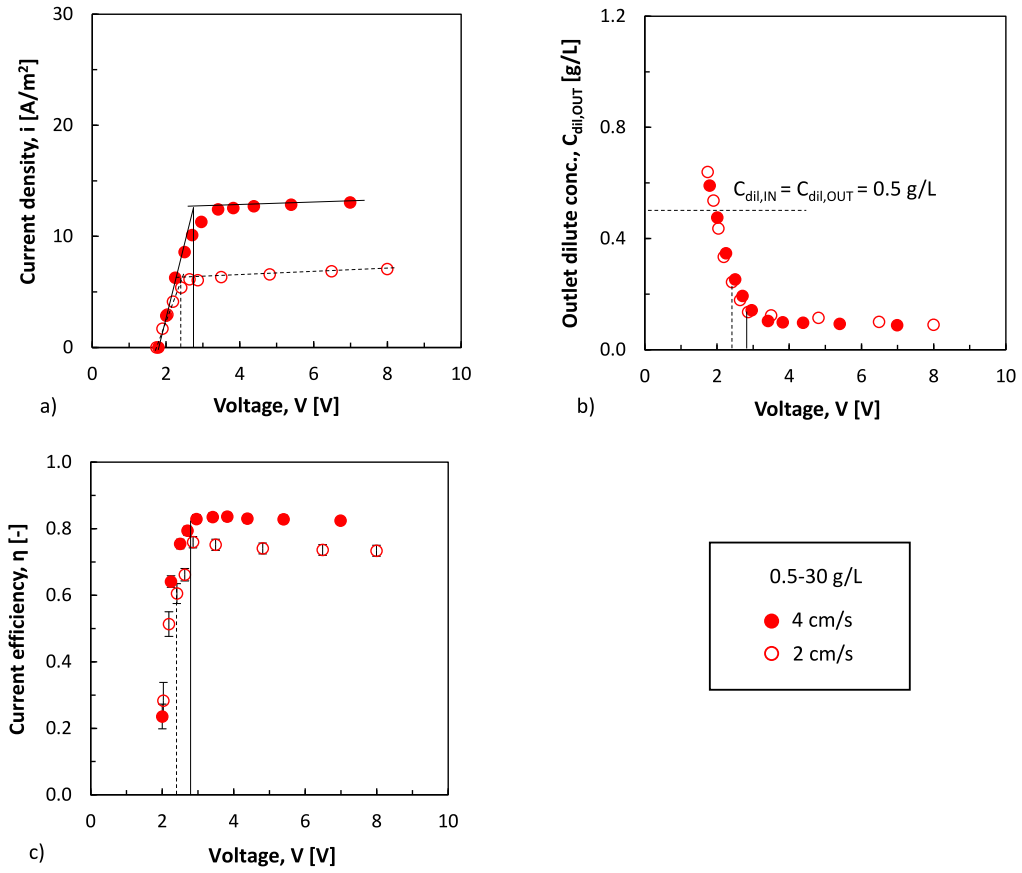

Fig. 4. a) Current density, b) diluate outlet concentration and c) current efficiency as functions of the applied voltage for tests performed at inlet concentrations of $C_{dil,IN} = 0.5$ g/L and $C_{conc,IN} = 30$ g/L and velocities of both solutions of either 4 cm/s or 2 cm/s. Dashed and continuous vertical lines identify the boundary between the first and the second region at 2 and 4 cm/s, respectively.

~0.06–0.09 g/L was measured for tests at $C_{dil,IN} = C_{conc,IN} = 0.5$ g/L.

3.2. CVCs of electrode segments

3.2.1. Feed concentrations 1–1 g/L

Fig. 5 reports the normalized CVC ($\widetilde{I}_i$ as function of $\widetilde{V}$) of each electrode couple, for tests performed with the inlet concentrations couple 1–1 g/L at velocities of 4 cm/s and 2 cm/s. The normalized CVC for the overall stack is also reported.

Interestingly, a very non-uniform current distribution was observed at any applied voltage. In the initial part of the first region of the overall CVC, the current increased linearly with the applied voltage in all four segments, albeit at a different rate (see the insets of Fig. 5). Even at low applied voltages, the measured current was highest at the first segment (adjacent to the feed inlet) and decreased through the following ones. For example, at $\widetilde{V} \sim 0.5$, i.e., in the middle of the first region, $\widetilde{I}_1$ was approximatively three times $\widetilde{I}_4$ or more. In other words, the current lines are much denser in a small portion of the stack close to the inlet. This behaviour can be explained from the Ohmic point of view by considering that the electrical resistance is inversely proportional to the electrolyte conductivity, which in turn is approximatively proportional to the concentration (below ~100 g/L) [14,77]. Therefore, the resistance reduction in the concentrate compartment does not compensate the resistance increase in the diluate compartment. Moreover, according to the IEM micro-heterogeneous model [34,35], the cell-pair resistance increases even more due to the increase in the membrane resistance. For these reasons, the current distribution became more uneven as the voltage was made to increase. The loss of linearity in the overall CVC, which started at $\widetilde{V} > 0.5$ (see the magnification of Fig. 5a), was caused by a slower increase of current in a portion of ~3/4 of the stack adjacent to the outlet (slope reduction in the CVCs of the electrode segments 2 to 4). At the "knee" of the overall stack CVC, the current distribution at the four segments started to change even more markedly. In fact, at the first electrode the current continued to increase (linearly even for a large range of $\widetilde{V}$), while at the other three electrodes it reached a maximum and then decreased. In the test carried out at 4 cm/s, the first maximum of current was reached at $\widetilde{V} \approx 0.8$ by the fourth segment, which was most affected by the reduced diluate conductivity. At $\widetilde{V}$ in the range of ~0.8–1.2, the current reached its maximum at the third and then at the second electrode. Similar values were observed for the test at 2 cm/s, where the maximum $\widetilde{I}_4$ was achieved at $\widetilde{V}$ of ~0.7, while the highest values of $\widetilde{I}_3$ and $\widetilde{I}_2$ were at $\widetilde{V}$ of ~0.8 and ~1.2.

In the second region of the overall CVC, the first stack segment exhibited a current increasing at a lower rate and tending to a maximum value. The maximum current density at the first electrode was ~88 A/m^2 and ~42 A/m^2 for 4 cm/s and 2 cm/s, respectively. Obviously, a distribution of the current occurred also within each segment, and in a narrow portion of stack close to the inlet the local current density probably reached much higher values. In contrast with the first segment, the other three exhibited a current decreasing as the voltage increased. The current eventually almost vanished in a large portion of the stack, i.e. a half (third and fourth electrode) in the test at 4 cm/s, or 3/4 (second to fourth electrode) in the test at 2 cm/s. A lower fluid velocity shortened the portion of the stack in the proximity of the inlet where the desalination effect was enhanced, while prolonging the remaining portion of the stack that contributed to a lesser extent (or even negligibly) to the desalination. In fact, the closer the CVC of the first electrode is to the overall CVC (particularly in its second region), the more current

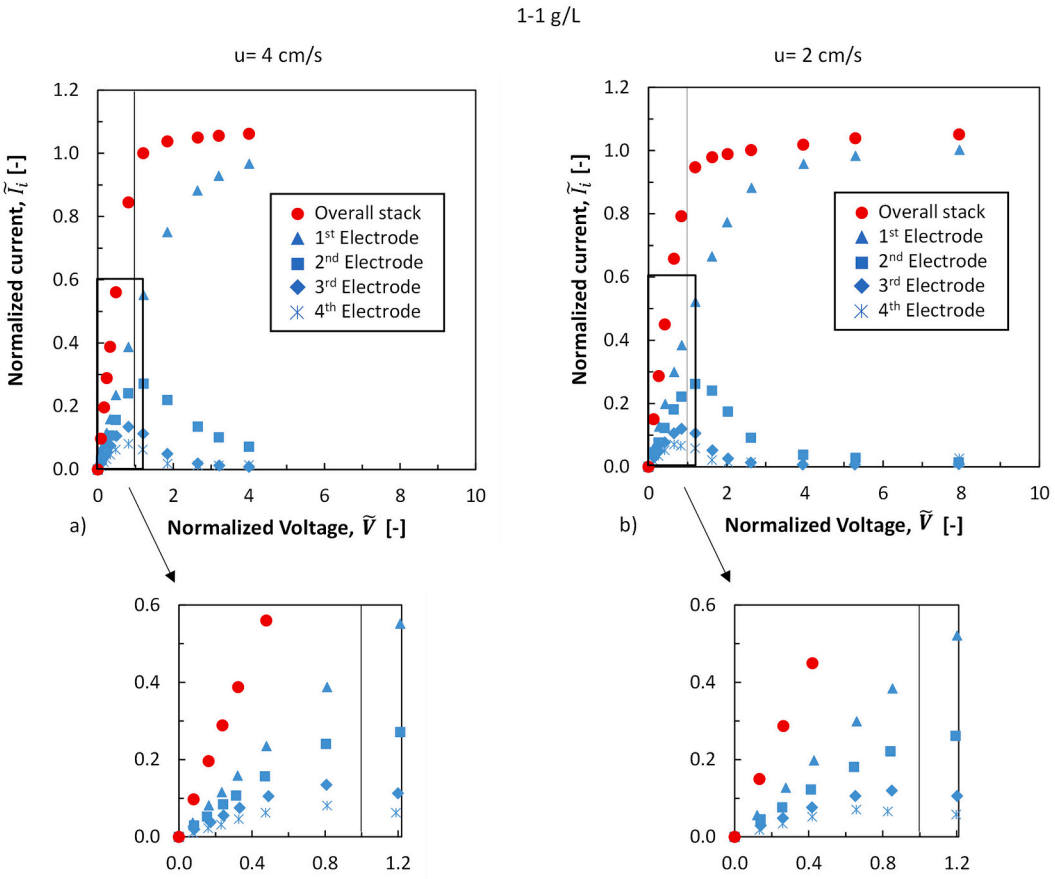

Fig. 5. Normalized CVCs of electrode segments for tests performed at velocities of a) 4 cm/s and b) 2 cm/s at inlet concentrations $C_{dil,IN} = C_{conc,IN} = 1$ g/L. The insets report magnifications at low values of normalized voltage. Normalized values were calculated by Eqs. (2) and (3). Vertical lines identify the boundary between the first and the second region ($\widetilde{V} = 1$).

is concentrated in the first part of the stack, making the remaining part unproductive and inefficient for desalination.

In the second region of the overall CVC ($\widetilde{V} > 1$), the normalized current $\widetilde{I}$ slightly increased above 1. This is not a strange result, as it reflects the fact that the current density of the entire stack slowly increased with respect to the LCD identified by the graphical "two tangents" method.

A possible interpretation of the plateau of the overall CVC could be related to the expansion of the limiting condition along the stack. At $\widetilde{V} \approx 1$, a local limiting condition could take place at the outlet, where the resistance (due to concentration polarization and lower conductivity) is the highest. As the voltage is increased, the limiting condition could extend backwards causing the overall CVC saturation and reflecting the development of the concentration profile in the diluate compartment (which will be shown in Section 3.3).

3.2.2. *Feed concentrations 0.5–30 g/L*

Fig. 6 reports the normalized CVCs[1] for tests performed with the inlet concentrations couple of 0.5–30 g/L at velocities of both solutions of 4 cm/s and 2 cm/s. By comparing Fig. 5 with Fig. 6, it is interesting to observe that the normalized CVCs were quite similar despite the inlet concentrations were changed from 1–1 g/L to 0.5–30 g/L. However, the high salinity gradient between the feed streams had some effects in the second region of the overall CVC. There, indeed, the current was low but did not approach zero in the last 2 or 3 segments at 4 or 2 cm/s, respectively, as it did in the case of 1–1 g/L, notwithstanding the flat profile of concentration. This can be attributed to the existence of important unwanted transport phenomena, which are enhanced by the high concentration gradient, counterbalancing the desalination effect of electrical current, leading to a higher local critical current density and lower current efficiency.

Such findings clearly indicate that the occurrence of the so called LCD condition in CVCs of long ED stacks could be effectively explained also looking only at the "Ohmic" behaviour (i.e., to the reduction of electrical conductivity) of an ED stack. Indeed, the concentration variation in the dilute channel leads to a significant variation in the local stack resistance and, hence, in the local current density (mal-)distribution. This results in the extremely high current densities occurring in the first portions of the stacks, leaving as practically non-operating the remaining part and generating the plateau region in the CVCs. A further analysis is continued also in the next section, where current and concentration distributions along the flow path are reported and commented.

Graphs for tests carried out at other inlet concentrations are provided in the Supplementary data (Figs. S4–S6), confirming the features of the CVCs discussed above.

3.3. *Distribution of electric current and of diluate concentration*

To better understand the distribution of current and of the interconnected desalination rate, Fig. 7 reports the current measured at each electrode segment over the total current, I_i/I_{tot}, and the estimated diluate concentration profile as functions of the longitudinal coordinate L, for

[1] Note that in our definition of normalized voltage (Eq. (3)) the OCV was subtracted from both the voltage and the limiting voltage, so that the normalized CVC starts from the origin.

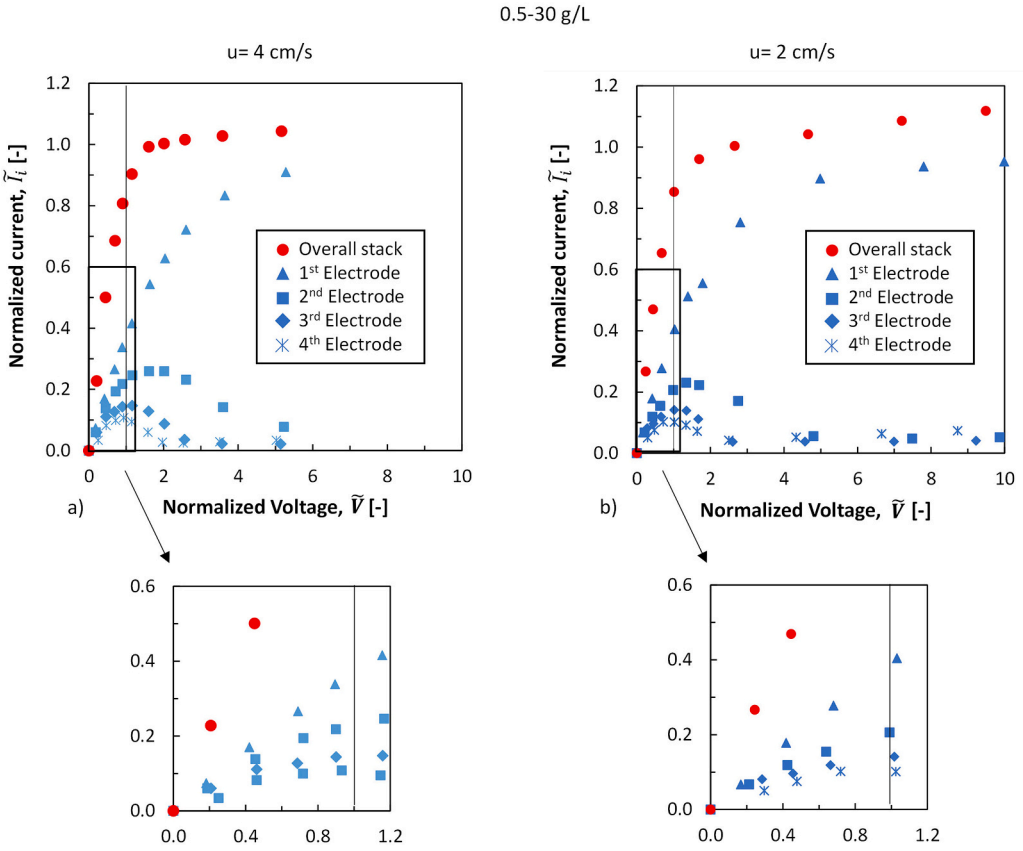

Fig. 6. Normalized CVCs of electrode segments for tests performed at velocities of a) 4 cm/s and b) 2 cm/s at inlet concentrations $C_{dil,IN} = 0.5$ g/L and $C_{conc,IN} = 30$ g/L. The insets report magnifications at low values of normalized voltage. Normalized values were calculated by Eqs. (2) and (3). Vertical lines identify the boundary between the first and the second region ($\widetilde{V} = 1$).

different values of normalized voltage $\widetilde{V}$ both below and above V_{lim}. Overall, it is confirmed that the electric current and the desalination rate were far from being uniformly distributed (ideal case with $I_i/I_{tot} = 25$ % for each segment i, and thus linear concentration profiles). The electric current and the desalination rate decreased (and the stack resistance increased) significantly along the stack at any applied voltage and for both the couples of inlet concentrations tested. As the voltage increased, I_i/I_{tot} and $C_{dil,IN,i} - C_{dil,OUT,i}$ were higher at the stack inlet. A clear distinction between the first quarter of the stack and the remaining part was observed. In fact, the current fraction increased roughly linearly (thus contributing substantially to the desalination process) in the first electrode. Conversely, the current fraction was significantly depleted in the remaining part of stack. The differences $C_{dil,IN,i} - C_{dil,OUT,i}$ are proportional to the measured current and, under the hypothesis of a uniform current efficiency, are those providing the concentration profiles reported in graph c and d of Fig. 7. In the test at 0.5–30 g/L inlet concentrations, the current distribution (and the distribution of the associated concentration gradient) in the longitudinal direction was slightly more uniform than at 1–1 g/L.

In the middle of the overall CVC's first region ($\widetilde{V} = 0.5$), the current fraction in the first quarter of the stack was 35–42 %, while it dropped to 11–16 % in the last quarter. At the limiting condition ($\widetilde{V} = 1$), which is of great practical interest for "traditional" ED operations, the first and fourth values of current fraction were 44–51 % and 8–12 %. The non-uniformity became stronger in the overall CVC's second region ($\widetilde{V} > 1$), arriving to concentrate 70–80 % of current in the first quarter of length and >90 % in the first half. The standard deviation of the current fraction distribution (STD) ranged from 0.11 to 0.33 at the extreme values of voltage selected for Fig. 7 ($\widetilde{V} = 0.5$ and $\widetilde{V} = 2.5$). For higher values of normalized voltage ($\widetilde{V} > 2.5$), the distribution was more uneven. For example, at $\widetilde{V} = 4$ the current fraction in the first quarter of the stack was 80–90 %, while <3 % was measured in the last electrode. The slightly higher uniformity of current distributions observed at 0.5–30 g/L compared with the test at 1–1 g/L results from lower useful currents. Indeed, by comparing the data series for the overall stack of Figs. 5 and 6, it can be observed that the current normalized by the limiting value is little affected by the inlet concentrations. In contrast, by comparing Figs. 3 and 4 it is evident that the LCD and the current efficiency are significantly lower at 0.5–30 g/L. Another different feature between the two tests performed with different inlet concentrations is that at 0.5–30 g/L the current in the second segment decreased less as a function of the applied voltage.

At $\widetilde{V} = 0.5$ and 1, the data series of current distribution reported in Fig. 7 are best fitted with quadratic laws, confirming previous theoretical results by Tanaka [62,81]. However, at higher voltage our experimental data are best fitted with exponential laws (or even a power law in one case). Despite parabolic trends could still provide good or best fitting within the limiting region, they are no longer realistic, as they presented a minimum preceding the last data point. Overall, by including all the data collected in this work (see the Supplementary data), there is not a unique equation suitable for fitting the current distribution as the operating conditions vary. Of course, we have only four points taken from as many electrode segments, so the "discretization degree" is rough. However, the feature of departing from the parabolic trend (which, to the best of the authors' knowledge is the only one mentioned in the literature) in favour of exponential or power laws is confirmed by several tests.

Regarding the concentration profile (Fig. 7, graph s c and d), the main difference between the two tests is that at 0.5–30 g/L the

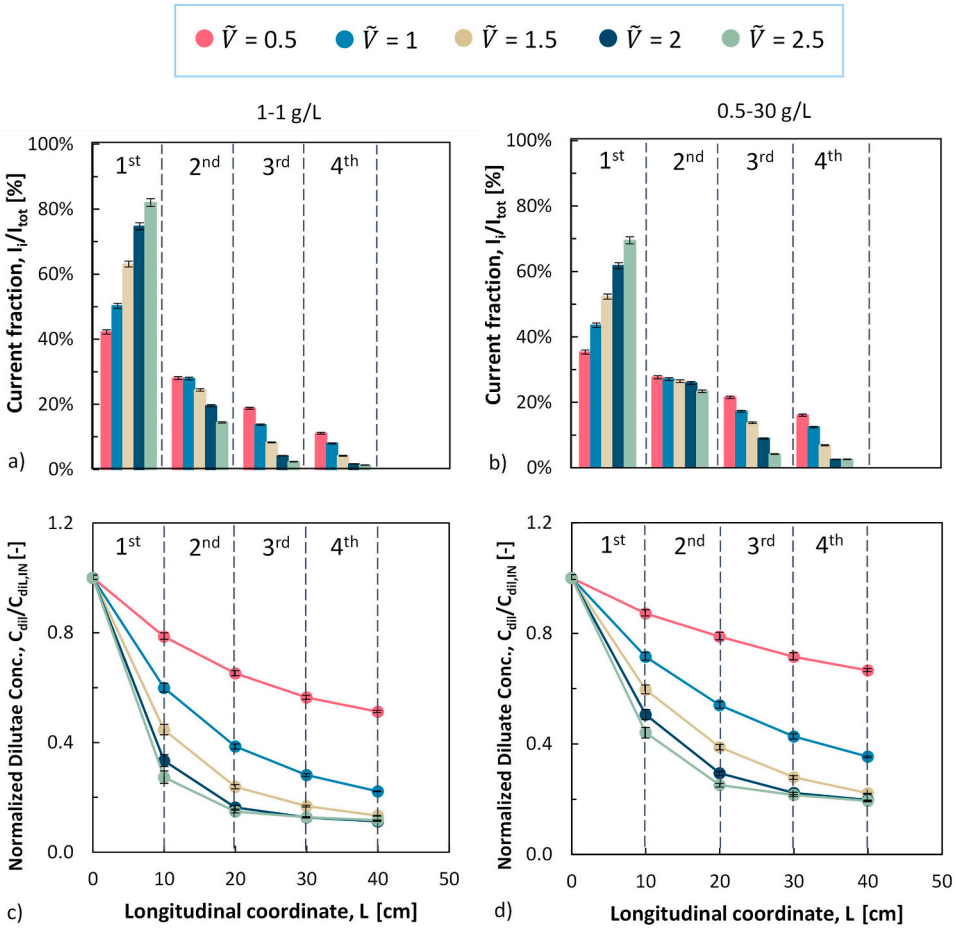

Fig. 7. Distribution of electrode current fraction I_i/I_{tot} (a and b) and normalized diluate concentration $C_{dil}/C_{dil,IN}$ (c and d) in the longitudinal direction at different $\tilde{V}$, for test performed at inlet concentrations of $C_{dil,IN} = C_{conc,IN} = 1$ g/L (a and c) and $C_{dil,IN} = 0.5$ g/L and $C_{conc,IN} = 30$ g/L (b and d), performed at 4 cm/s.

desalination rate is lower than at 1–1 g/L for any $\tilde{V}$, since the former test case was characterized by lower values of both current and current efficiency, as mentioned above.

An important feature of the decreasing concentration profiles in the diluate compartment is their concavity is directly upwards, which implies the occurrence of an average concentration closer to the outlet value. As a result, the average electrical resistance is higher, and increases rapidly with the applied voltage. This result points out the relevance of being aware of the current distribution in order to select cost-optimal operating conditions and ED design features for desalination.

The feedwater velocity was poorly relevant to the current fraction distribution measured for any normalized voltage, thus experimental results at 2 cm/s are not reported here for the sake of brevity. These results, as well as those regarding other inlet concentrations couples for both velocities, are reported in detail in the Supplementary data (Figs. S7–S11).

3.4. Comparison of all tests

By comparing some representative results from all tests, this subsection aims at providing an evaluation of the effect of the operating conditions (inlet concentrations and velocity) on the outcomes of the experimental campaign. To this purpose, Table 3 reports the values of the stack apparent resistance at $i \rightarrow 0$, LCD, and average current efficiency (calculated for experimental points at $\tilde{V} > 0$).

The Ohmic stack resistance, R, varied from 0.036 Ω m^2 (1–60 g/L inlet concentrations, 4 cm/s) to 0.208 Ω m^2 (0.5–0.5 g/L inlet concentrations, 2 cm/s). The increase in velocity (from 2 cm/s to 4 cm/s) resulted in the reduction of resistance (up to ~40 %) due to the lower desalination effect, produced by the larger residence time. As can be expected, an increase in the inlet concentration of either the diluate $C_{dil,IN}$ (from 0.5 g/L to 1 g/L) or the concentrate $C_{conc,IN}$ (from 0.5 g/L to 30 g/L, and from 1 g/L to 30 g/L or 60 g/L) resulted in a significant reduction in stack resistance.

The LCD was comprised between ~5.5 and ~27.3 A m^{-2}, confirming the roughly proportional influence of both the flow rate (or velocity) and $C_{dil,IN}$. A modest increase in LCD with $C_{conc,IN}$ was found, as already observed in previous experiments with shorter stacks [74,79].

The linear velocity had a mild influence on the average current efficiency, and it produced a positive effect in most cases. The average η was 92–95 % for tests at equal inlet concentrations, while the presence of a high salinity solution (seawater at 30 g/L or concentrated seawater at 60 g/L) in the concentrate compartment made it drop up to a minimum value of 62 % due to the detrimental effect of unwanted transport

Table 3
Excerpt of some synthetic results for all the operating conditions tested.

	R at $i \rightarrow 0$ [Ω m^2]		LCD [A/m^2]		Average η (at $\tilde{V} > 0$)	
	4 cm/s	2 cm/s	4 cm/s	2 cm/s	4 cm/s	2 cm/s
0.5–0.5 g/L	0.139	0.208	11.5	5.5	0.95	0.93
0.5–30 g/L	0.073	0.096	12.5	6.3	0.74	0.64
1–1 g/L	0.090	0.095	22.6	10.6	0.92	0.94
1–30 g/L	0.040	0.066	23.5	11.5	0.84	0.80
1–60 g/L	0.036	0.046	27.3	15.6	0.69	0.62

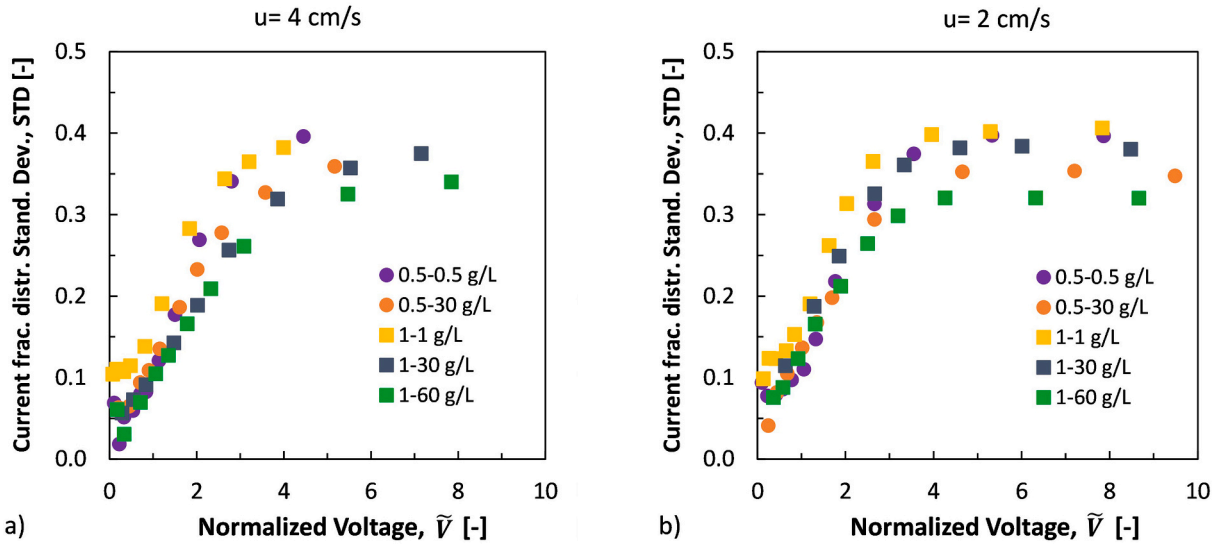

Fig. 8. Standard deviation of the distribution of current as a function of the normalized voltage for tests performed at velocities of a) 4 cm/s and b) 2 cm/s.

phenomena. Of course, $C_{conc,IN}$ had a great influence on η. In addition, the current efficiency increased also as $C_{dil,IN}$ increased.

Fig. 8 reports the parameter chosen as representative of current (mal) distribution, i.e., its STD.

The STD of the current fraction distribution among the four-segment electrodes ranged from near-zero values to a maximum of 0.41 ($\widetilde{V} = 7.8$, 1–1 g/L, 2 cm/s), depending on the operating conditions adopted. The STD increased quite linearly as the normalized voltage increased up to ~4. Then, the STD settled to almost constant values. The linear velocity had a modest effect on the current distribution, and it was positive (i.e., the STD was slightly reduced as the velocity was increased from 2 cm/s to 4 cm/s) in most cases. Similarly, by changing the inlet concentrations, the STD was moderately affected. A higher $C_{conc,IN}$ reduced STD in most cases; a higher $C_{dil,IN}$ increased STD at 2 cm/s and reduced it at 4 cm/s. By focusing on the data of current distribution at $\widetilde{V} = 1$, which can be considered the operating voltage of the greatest interest for conventional ED processes, the STD ranged from 0.10 to 0.17. In relative terms, these values of STD were 40 % and 68 %, respectively, of the average current fraction (0.25), raising a clear warning on the current maldistribution in typical ED operations.

4. Conclusions

This work provided a detailed quantification of the non-uniform current distribution along the stack across the first and the second region of the CVC via experimental measurements. Although distribution phenomena have been known, and multi-stage ED configurations have been devised to deal with them, the results of this study highlight that the stages of industrial plants, which have a path length in the order of 1 m, still suffer from issues of current maldistribution.

The CVCs of the four segments exhibited an initial linear increase, but with a slope decreasing from the 1st to the 4th segment, showing that even at $I_{tot} \rightarrow 0$ the current was not uniform. In the 1st segment the current continued to increase until a plateau was reached approaching that of the overall CVC. In contrast, in the other three segments it reached a maximum straddling the boundary of the first and the second region of the overall CVC, with the voltage at current maximum increasing in the order $4^{th} < 3^{rd} < 2^{nd}$.

The current fraction (I_i/I_{tot}) decreased from inlet to outlet (i.e., from segment 1 to 4) and its distribution was more uneven as the voltage increased. In the first region of the overall CVC, I_1/I_{tot} was up to ~50 %. As the normalized voltage $\widetilde{V}$ increased, I_1/I_{tot} increased linearly or oven more than linearly up to 80–90 %, while in the other segments I_i/I_{tot} decreased towards low or even negligible values in the limiting region. The measured current trends were well fitted by quadratic laws in the overall CVC's first region, and by exponential or power laws in its second region. The fluid velocity and the inlet concentrations had a moderate effect on the current distribution. As $\widetilde{V}$ increased, the standard deviation of the current fraction distribution (STD) increased up to 0.41. At $\widetilde{V} = 1$, representative of industrial operations, the values of STD ranged from 40 % to 68 % of the average current fraction (0.25), thus clearly indicating the occurrence of a severe maldistribution problem.

The current distribution, characterized by its accumulation in a portion of stack adjacent to the inlet (where most desalination takes place), is intrinsically related to the concentration distribution. Diluate concentration profiles had their concavity upwards, meaning that the desalination rate decreased along the path, and indicating the increase of both local and average resistances, with amplified effects as the applied voltage increases. CVC as a whole, LCD, current efficiency and SEC will be affected by the intertwined combination of the distributions arising from the desalination effect.

Future research should focus on the evaluation of the total resistance and all its contributions for a thorough understanding of the stack behaviour, especially in the limiting region. This will make a clear distinction between the desalination effect and other phenomena, including concentration polarization and water dissociation.

Abbreviations

Acronyms

AEM	anion exchange membrane
CCD	critical current density
CEM	cation exchange membrane
CVC	current-voltage curve
ED	electrodialysis
ERS	electrode rinse solution
IEC	ion-exchange capacity
IEM	ion-exchange membrane
LCD	limiting current density
MMO	mixed metal oxide
OCV	open circuit voltage
RED	reverse electrodialysis
RO	reverse osmosis
SEC	specific energy consumption

Symbols

C	concentration [g/L]
F	Faraday constant [C/mol]
I	current [A]
i	current density [A/m^2]
$\widetilde{I}$	normalized current
L	longitudinal coordinate along the stack length [cm]
M_w	NaCl molecular weight [g/mol]
N_{CP}	cell pair number
Q	flowrate [L/s]
R	electrical areal resistance [Ω m^2]
STD	standard deviation (of electric current distribution)
V	voltage [V]
$\widetilde{V}$	normalized voltage
z	ion valence

Greek symbols

η	current efficiency

Subscripts and superscripts

AVE	average
conc	concentrate
CP	cell pair
dil	diluate
i	i-th segment
IN	inlet
lim	limiting
OUT	outlet
tot	total

CRediT authorship contribution statement

Antonia Filingeri: Validation, Formal analysis, Investigation, Data curation, Writing – original draft, Visualization. **Luigi Gurreri:** Validation, Formal analysis, Data curation, Methodology, Writing – original draft, Writing – review & editing, Visualization. **Michele Ciofalo:** Conceptualization, Methodology, Writing – review & editing, Supervision, Project administration. **Andrea Cipollina:** Conceptualization, Methodology, Resources, Writing – review & editing, Supervision, Project administration, Funding acquisition. **Alessandro Tamburini:** Conceptualization, Methodology, Resources, Writing – review & editing, Supervision, Project administration, Funding acquisition. **Giorgio Micale:** Conceptualization, Methodology, Resources, Writing – review & editing, Supervision, Project administration, Funding acquisition.

Declaration of competing interest

The authors declare that they have no known competing financial interests or personal relationships that could have appeared to influence the work reported in this paper.

Data availability

The data that has been used is confidential.

Acknowledgments

The authors are grateful to REDstack B.V. for supplying the ED stack and to Fujifilm Manufacturing Europe B.V. for supplying all the membranes for this study.

Part of this research was supported by *Piano di incentivi per la ricerca di Ateneo 2020/2022 (Pia.ce.ri.) Linea 2D* - University of Catania.

Appendix A. Supplementary data

Supplementary data to this article can be found online at https://doi.org/10.1016/j.desal.2023.116541.

References

[1] A. Campione, L. Gurreri, M. Ciofalo, G. Micale, A. Tamburini, A. Cipollina, Electrodialysis for water desalination: a critical assessment of recent developments on process fundamentals, models and applications, Desalination 434 (2018) 121–160, https://doi.org/10.1016/j.desal.2017.12.044.

[2] L. Bazinet, T.R. Geoffroy, Electrodialytic processes: market overview, membrane phenomena, recent developments and sustainable strategies, Membranes 10 (2020) 1–72, https://doi.org/10.3390/membranes10090221 (Basel).

[3] L. Gurreri, A. Tamburini, A. Cipollina, G. Micale, Electrodialysis applications in wastewater treatment for environmental protection and resources recovery: a systematic review on progress and perspectives, Membranes 10 (2020) 1–93, https://doi.org/10.3390/membranes10070146 (Basel).

[4] F.E. Ahmed, A. Khalil, N. Hilal, Emerging desalination technologies: current status, challenges and future trends, Desalination 517 (2021), 115183, https://doi.org/10.1016/j.desal.2021.115183.

[5] J. Eke, A. Yusuf, A. Giwa, A. Sodiq, The global status of desalination: an assessment of current desalination technologies, plants and capacity, Desalination 495 (2020), 114633, https://doi.org/10.1016/j.desal.2020.114633.

[6] W. Li, W.B. Krantz, E.R. Cornelissen, J.W. Post, A.R.D. Verliefde, C.Y. Tang, A novel hybrid process of reverse electrodialysis and reverse osmosis for low energy seawater desalination and brine management, Appl. Energy 104 (2013) 592–602, https://doi.org/10.1016/j.apenergy.2012.11.064.

[7] M. La Cerva, L. Gurreri, A. Cipollina, A. Tamburini, M. Ciofalo, G. Micale, Modelling and cost analysis of hybrid systems for seawater desalination: electromembrane pre-treatments for reverse osmosis, Desalination 467 (2019) 175–195, https://doi.org/10.1016/j.desal.2019.06.010.

[8] L. Gurreri, M. La Cerva, J. Moreno, B. Goossens, A. Trunz, A. Tamburini, Coupling of electromembrane processes with reverse osmosis for seawater desalination: pilot plant demonstration and testing, Desalination 526 (2022), 115541, https://doi.org/10.1016/j.desal.2021.115541.

[9] V.V. Wagholikar, H. Zhuang, N.E. Moe, J. Barber, H. Ramanan, J.Y.H. Fuh, Analysis of RED/dRED stack performance using a resistances in series model, Desalination 496 (2020), 114505, https://doi.org/10.1016/j.desal.2020.114505.

[10] M. Philibert, A. Filingeri, C. Natalello, N. Moe, E. Filloux, A. Cipollina, Surface water RO permeate remineralization through minerals recovery from brines, Desalination 531 (2022), 115725, https://doi.org/10.1016/j.desal.2022.115725.

[11] K.M. Chehayeb, K.G. Nayar, J.H. Lienhard, On the merits of using multi-stage and counterflow electrodialysis for reduced energy consumption, Desalination 439 (2018) 1–16, https://doi.org/10.1016/j.desal.2018.03.026.

[12] A. Campione, A. Cipollina, I.D.L. Bogle, L. Gurreri, A. Tamburini, M. Tedesco, G. Micale, A hierarchical model for novel schemes of electrodialysis desalination, Desalination 465 (2019) 79–93, https://doi.org/10.1016/j.desal.2019.04.020.

[13] M.M. Generous, N.A.A. Qasem, S.M. Zubair, The significance of modeling electrodialysis desalination using multi-component saline water, Desalination 496 (2020), 114347, https://doi.org/10.1016/j.desal.2020.114347.

[14] G. Battaglia, L. Gurreri, M. Ciofalo, A. Cipollina, I.D.L. Bogle, A. Pirrotta, G. Micale, A 2-D model of electrodialysis stacks including the effects of membrane deformation, Desalination 500 (2021), 114835, https://doi.org/10.1016/j.desal.2020.114835.

[15] A.H. Galama, M. Saakes, H. Bruning, H.H.M. Rijnaarts, J.W. Post, Seawater predesalination with electrodialysis, Desalination 342 (2014) 61–69, https://doi.org/10.1016/j.desal.2013.07.012.

[16] G.J. Doornbusch, M. Tedesco, J.W. Post, Z. Borneman, K. Nijmeijer, Experimental investigation of multistage electrodialysis for seawater desalination, Desalination 464 (2019) 105–114, https://doi.org/10.1016/j.desal.2019.04.025.

[17] G.J. Doornbusch, M. Bel, M. Tedesco, J.W. Post, Z. Borneman, K. Nijmeijer, Effect of membrane area and membrane properties in multistage electrodialysis on seawater desalination performance, J. Membr. Sci. 611 (2020), 118303, https://doi.org/10.1016/j.memsci.2020.118303.

[18] R.K. McGovern, S.M. Zubair, J.H. Lienhard V, The cost effectiveness of electrodialysis for diverse salinity applications, Desalination 348 (2014) 57–65, https://doi.org/10.1016/j.desal.2014.06.010.

[19] H.J. Lee, H. Strathmann, S.H. Moon, Determination of the limiting current density in electrodialysis desalination as an empirical function of linear velocity, Desalination 190 (2006) 43–50, https://doi.org/10.1016/j.desal.2005.08.004.

[20] V.M. Barragán, C. Ruíz-Bauzá, Current-voltage curves for ion-exchange membranes: a method for determining the limiting current density, J. Colloid Interface Sci. 205 (1998) 365–373, https://doi.org/10.1006/jcis.1998.5649.

[21] J.J. Krol, M. Wessling, H. Strathmann, Concentration polarization with monopolar ion exchange membranes: current-voltage curves and water dissociation, J. Membr. Sci. 162 (1999) 145–154, https://doi.org/10.1016/S0376-7388(99)00133-7.

[22] M.S. Isaacson, A.A. Sonin, Sherwood number and friction factor correlations for electrodialysis systems, with application to process optimization, Ind. Eng. Chem. Process. Des. Dev. 15 (1976) 313–321, https://doi.org/10.1021/i260058a017.

[23] W.J. Koros, Y.H. Ma, T. Shimidzu, Terminology for membranes and membrane processes (IUPAC Recommendations 1996), Pure Appl. Chem. 68 (1996) 1479–1489, https://doi.org/10.1351/pac199668071479.

[24] V.V. Nikonenko, N.D. Pismenskaya, E.I. Belova, P. Sistat, P. Huguet, G. Pourcelly, C. Larchet, Intensive current transfer in membrane systems: modelling, mechanisms and application in electrodialysis, Adv. Colloid Interf. Sci. 160 (2010) 101–123, https://doi.org/10.1016/j.cis.2010.08.001.
[25] T.L. Hill, G. Scatchard, B.A. Pethica, I.J. Straub, R. Schlögl, G. Manecke, R. Schlögl, M. Nagasawa, I. Kagawa, P. Meares, K. Sollner, F.L. Tye, A. Despiá, G.J. Hills, F. Helfferich, J.E. Salmon, R.J.P. Williams, A.M. Peers, F. Bergsma, A.J. Staverman, N. Krishnaswamy, F. Runge, F. Wolf, E. Glueckauf, D. Reichenberg, R. Neihof, R. D. Keynes, A.R. Ubbelohde, R.M. Barrer, General discussion, Discuss. Faraday Soc. 21 (1956) 117–140, https://doi.org/10.1039/DF9562100117.
[26] R. Kunin, Ion Exchange, McGraw-Hill, N. Y., 1960, https://doi.org/10.1021/ac60161a609.
[27] V.G. Levich, C.W. Tobias, Physicochemical Hydrodynamics, Prentice-Hall, Englewood Cliffs, N.J., 1963, https://doi.org/10.1149/1.2425619.
[28] C. Tian, K.R. Kristiansen, S. Kjelstrup, V.M. Barragán, Two methods for determination of transport numbers in ion-exchange membranes, Int. J. Thermophys. 43 (2022) 1–19, https://doi.org/10.1007/s10765-021-02939-1.
[29] Y. Freijanes, V.M. Barragán, S. Muñoz, Chronopotentiometric study of a nafion membrane in presence of glucose, J. Membr. Sci. 510 (2016) 79–90, https://doi.org/10.1016/j.memsci.2016.02.054.
[30] V.M. Barragán, C. Ruíz Bauzá, Current-voltage curves for a cation-exchange membrane in methanol-water electrolyte solutions, J. Colloid Interface Sci. 247 (2002) 138–148, https://doi.org/10.1006/jcis.2001.8065.
[31] F. Stockmeier, M. Schatz, M. Habermann, J. Linkhorst, A. Mani, M. Wessling, Direct 3D observation and unraveling of electroconvection phenomena during concentration polarization at ion-exchange membranes, J. Membr. Sci. 640 (2021), 119846, https://doi.org/10.1016/j.memsci.2021.119846.
[32] J.J. Krol, M. Wessling, H. Strathmann, Chronopotentiometry and overlimiting ion transport through monopolar ion exchange membranes, J. Membr. Sci. 162 (1999) 155–164, https://doi.org/10.1016/S0376-7388(99)00134-9.
[33] M.K. Urtenov, A.M. Uzdenova, A.V. Kovalenko, V.V. Nikonenko, N. D. Pismenskaya, V.I. Vasil'eva, P. Sistat, G. Pourcelly, Basic mathematical model of overlimiting transfer enhanced by electroconvection in flow-through electrodialysis membrane cells, J. Membr. Sci. 447 (2013) 190–202, https://doi.org/10.1016/j.memsci.2013.07.033.
[34] C. Larchet, S. Nouri, B. Auclair, L. Dammak, V. Nikonenko, Application of chronopotentiometry to determine the thickness of diffusion layer adjacent to an ion-exchange membrane under natural convection, Adv. Colloid Interf. Sci. 139 (2008) 45–61, https://doi.org/10.1016/j.cis.2008.01.007.
[35] J. Veerman, The effect of the NaCl bulk concentration on the resistance of ion exchange membranes-measuring and modeling, Energies 13 (2020), https://doi.org/10.3390/en13081946.
[36] Q.-B. Chen, Y. Xu, P.-F. Li, J. Wang, L. Dong, J. Zhao, J. Wang, An emerging pilot-scale electrodialysis system for desalination of SWNF permeate: evaluating the role of typical factors, Desalination 542 (2022), 116064, https://doi.org/10.1016/j.desal.2022.116064.
[37] K.J. Min, E.J. Oh, G. Kim, J.H. Kim, J.H. Ryu, K.Y. Park, Influence of linear flow velocity and ion concentration on limiting current density during electrodialysis, Desalin. Water Treat. 175 (2020) 334–340, https://doi.org/10.5004/dwt.2020.24663.
[38] A. Rajput, J. Sharma, S.K. Raj, V. Kulshrestha, Dehydrofluorinated poly(vinylidene fluoride-co-hexafluoropropylene) based crosslinked cation exchange membrane for brackish water desalination via electrodialysis, Colloids Surf.A Physicochem. Eng. Asp. 630 (2021), https://doi.org/10.1016/j.colsurfa.2021.127576.
[39] R. Valerdi-Pérez, J. Ibáez-Mengual, Current-voltage curves for an electrodialysis reversal pilot plant: determination of limiting currents, Desalination 141 (2001) 23–37, https://doi.org/10.1016/S0011-9164(01)00386-1.
[40] G. Doornbusch, M. van der Wal, M. Tedesco, J. Post, K. Nijmeijer, Z. Borneman, Multistage electrodialysis for desalination of natural seawater, Desalination 505 (2021), 114973, https://doi.org/10.1016/j.desal.2021.114973.
[41] G. Doornbusch, H. Swart, M. Tedesco, J. Post, Z. Borneman, K. Nijmeijer, Current utilization in electrodialysis: electrode segmentation as alternative for multistaging, Desalination 480 (2020), 114243, https://doi.org/10.1016/j.desal.2019.114243.
[42] F. Giacalone, P. Catrini, L. Gurreri, A. Tamburini, A. Cipollina, G. Micale, A. Piacentino, Exergy analysis of electrodialysis for water desalination: influence of irreversibility sources, Energy Convers. Manag. 258 (2022), 115314, https://doi.org/10.1016/j.enconman.2022.115314.
[43] C. Simões, D. Pintossi, M. Saakes, W. Brilman, Optimizing multistage reverse electrodialysis for enhanced energy recovery from river water and seawater: experimental and modeling investigation, Adv. Appl. Energy 2 (2021), https://doi.org/10.1016/j.adapen.2021.100023.
[44] J. Veerman, Reverse electrodialysis: co-and counterflow optimization of multistage configurations for maximum energy efficiency, Membranes 10 (2020) 1–13, https://doi.org/10.3390/membranes10090206 (Basel).
[45] C. Simões, D. Pintossi, M. Saakes, Z. Borneman, W. Brilman, K. Nijmeijer, Electrode segmentation in reverse electrodialysis: improved power and energy efficiency, Desalination 492 (2020), 114604, https://doi.org/10.1016/j.desal.2020.114604.
[46] J. Veerman, M. Saakes, S.J. Metz, G.J. Harmsen, Reverse electrodialysis: a validated process model for design and optimization, Chem. Eng. J. 166 (2011) 256–268, https://doi.org/10.1016/j.cej.2010.10.071.
[47] J. Veerman, M. Saakes, S.J. Metz, G.J. Harmsen, Electrical power from sea and river water by reverse electrodialysis: a first step from the laboratory to a real power plant, Environ. Sci. Technol. 44 (2010) 9207–9212, https://doi.org/10.1021/es1009345.
[48] A. Culcasi, L. Gurreri, G. Micale, A. Tamburini, Bipolar membrane reverse electrodialysis for the sustainable recovery of energy from pH gradients of industrial wastewater: performance prediction by a validated process model, J. Environ. Manag. 287 (2021), 112319, https://doi.org/10.1016/j.jenvman.2021.112319.
[49] M. Geske, M. Heuer, G. Heideck, Z.A. Styczynski, Current density distribution mapping in PEM fuel cells as an instrument for operational measurements, Energies 3 (2010) 770–783, https://doi.org/10.3390/en3040770.
[50] M. Noponen, T. Mennola, M. Mikkola, T. Hottinen, P. Lund, Measurement of current distribution in a free-breathing PEMFC, J. Power Sources 106 (2002) 304–312, https://doi.org/10.1016/S0378-7753(01)01063-1.
[51] A. Bhattarai, N. Wai, R. Schweiss, A. Whitehead, G.G. Scherer, P.C. Ghimire, T. D. Nguyen, H.H. Hng, Study of flow behavior in all-vanadium redox flow battery using spatially resolved voltage distribution, J. Power Sources 360 (2017) 443–452, https://doi.org/10.1016/j.jpowsour.2017.06.039.
[52] J.T. Clement, D.S. Aaron, M.M. Mench, In situ localized current distribution measurements in all-vanadium redox flow batteries, J. Electrochem. Soc. 163 (2016) A5220–A5228, https://doi.org/10.1149/2.0241601jes.
[53] W. Jiang, L. Lin, X. Xu, H. Wang, P. Xu, Physicochemical and electrochemical characterization of cation-exchange membranes modified with polyethyleneimine for elucidating enhanced monovalent permselectivity of electrodialysis, J. Membr. Sci. 572 (2019) 545–556, https://doi.org/10.1016/j.memsci.2018.11.038.
[54] C.C.N. Kunrath, D.C. Patrocínio, M.A. Siqueira Rodrigues, T. Benvenuti, F.D. R. Amado, Electrodialysis reversal as an alternative treatment for producing drinking water from brackish river water: a case study in the dry season, northeastern Brazil, J. Environ. Chem. Eng. 8 (2020), 103719, https://doi.org/10.1016/j.jece.2020.103719.
[55] X. Xu, Q. He, G. Ma, H. Wang, N. Nirmalakhandan, P. Xu, Pilot demonstration of reclaiming municipal wastewater for irrigation using electrodialysis reversal: effect of operational parameters on water quality, Membranes 11 (2021), https://doi.org/10.3390/membranes11050333 (Basel).
[56] X. Xu, Q. He, G. Ma, H. Wang, N. Nirmalakhandan, P. Xu, Selective separation of mono- and di-valent cations in electrodialysis during brackish water desalination: bench and pilot-scale studies, Desalination 428 (2018) 146–160, https://doi.org/10.1016/j.desal.2017.11.015.
[57] K. Knežević, D. Reif, M. Harasek, J. Krampe, N. Kreuzinger, Assessment of graphical methods for determination of the limiting current density in complex electrodialysis-feed solutions, Membranes 12 (2022), https://doi.org/10.3390/membranes12020241 (Basel).
[58] N. van Linden, H. Spanjers, J.B. van Lier, Application of dynamic current density for increased concentration factors and reduced energy consumption for concentrating ammonium by electrodialysis, Water Res. 163 (2019), 114856, https://doi.org/10.1016/j.watres.2019.114856.
[59] W. He, A.C. Le Henaff, S. Amrose, T. Buonassisi, I.M. Peters, A.G. Winter, Voltage- and flow-controlled electrodialysis batch operation: flexible and optimized brackish water desalination, Desalination 500 (2020), 114837, https://doi.org/10.1016/j.desal.2020.114837.
[60] A.A. Sonin, R.F. Probstein, A hydrodynamic theory of desalination by electrodialysis, Desalination 5 (1968) 293–329, https://doi.org/10.1016/S0011-9164(00)80105-8.
[61] G. Grossman, A.A. Sonin, Experimental study of the effects of hydrodynamics and membrane fouling in electrodialysis, Desalination 10 (1972) 157–180, https://doi.org/10.1016/S0011-9164(00)80084-3.
[62] Y. Tanaka, Current density distribution, limiting current density and saturation current density in an ion-exchange membrane electrodialyzer, J. Membr. Sci. 210 (2002) 65–75, https://doi.org/10.1016/S0376-7388(02)00376-9.
[63] Y. Tanaka, Simulation of an ion exchange membrane electrodialysis process for continuous saline water desalination, Desalin. Water Treat. 22 (2010) 271–285, https://doi.org/10.5004/dwt.2010.1858.
[64] Y. Tanaka, A computer simulation of continuous ion exchange membrane electrodialysis for desalination of saline water, Desalination 249 (2009) 809–821, https://doi.org/10.1016/j.desal.2009.04.011.
[65] Y. Tanaka, A computer simulation of batch ion exchange membrane electrodialysis for desalination of saline water, Desalination 249 (2009) 1039–1047, https://doi.org/10.1016/j.desal.2009.06.055.
[66] A. Ghorbani, A. Ghassemi, Brackish water desalination using electrodialysis: predictive mass transfer and concentration distribution model along the electrodialyzer, Water Sci. Technol. 77 (2018) 597–607, https://doi.org/10.2166/wst.2017.547.
[67] Y. Tanaka, Ion-exchange membrane electrodialysis of saline water and its numerical analysis, Ind. Eng. Chem. Res. 50 (2011) 10765–10777, https://doi.org/10.1021/ie2005498.
[68] K. Mitko, M. Turek, Concentration distribution along the electrodialyzer, Desalination 341 (2014) 94–100, https://doi.org/10.1016/j.desal.2014.02.040.
[69] M. Turek, K. Mitko, Residence time distribution of the electrodialyzer under electric field conditions, Desalination 342 (2014) 139–147, https://doi.org/10.1016/j.desal.2013.11.042.
[70] L. Gurreri, M. Ciofalo, A. Cipollina, A. Tamburini, G. Micale, Application of computational fluid dynamics technique in electrodialysis/reverse electrodialysis processes, in: A. Basile, K. Ghasemzadeh (Eds.), Curr. Trends Futur. Dev. Membr, Elsevier, 2022, pp. 81–160, https://doi.org/10.1016/B978-0-12-822294-2.00011-4.
[71] I. El Mokhtar, L. Gurreri, A. Tamburini, A. Cipollina, M. Ciofalo, S. al T. Bouguecha, G. Micale, CFD prediction of flow, heat and mass transfer in woven spacer-filled channels for membrane processes, Int. J. Heat Mass Transf. 173 (2021), 121246, https://doi.org/10.1016/j.ijheatmasstransfer.2021.121246.

[72] L. Gurreri, A. Tamburini, A. Cipollina, G. Micale, M. Ciofalo, Pressure drop at low Reynolds numbers in woven-spacer-filled channels for membrane processes: CFD prediction and experimental validation, Desalin. Water Treat. 61 (2017) 170–182, https://doi.org/10.5004/dwt.2016.11279.
[73] E.V. Laktionov, N.D. Pismenskaya, V.V. Nikonenko, V.I. Zabolotsky, Method of electrodialysis stack testing with the feed solution concentration regulation, Desalination 151 (2003) 101–116, https://doi.org/10.1016/S0011-9164(02)00988-8.
[74] M. La Cerva, L. Gurreri, M. Tedesco, A. Cipollina, M. Ciofalo, A. Tamburini, G. Micale, Determination of limiting current density and current efficiency in electrodialysis units, Desalination 445 (2018) 138–148, https://doi.org/10.1016/j.desal.2018.07.028.
[75] S.S. Islam, R.L. Gupta, K. Ismail, Extension of the Falkenhagen-Leist–Kelbg equation to the electrical conductance of concentrated aqueous electrolytes, J. Chem. Eng. Data 36 (1991) 102–104, https://doi.org/10.1021/je00001a031.
[76] A.A. Clifford, Multivariate error analysis; a handbook of error propagation and calculation in many-parameter systems 112, 1973 http://seismo.berkeley.edu/~kirchner/eps_120/Toolkits/Toolkit_05.pdf.
[77] M.L. La Cerva, M. Di Liberto, L. Gurreri, A. Tamburini, A. Cipollina, G. Micale, M. Ciofalo, Coupling CFD with a one-dimensional model to predict the performance of reverse electrodialysis stacks, J. Membr. Sci. 541 (2017) 595–610, https://doi.org/10.1016/j.memsci.2017.07.030.
[78] D.A. Vermaas, M. Saakes, K. Nijmeijer, Power generation using profiled membranes in reverse electrodialysis, J. Membr. Sci. 385–386 (2011) 234–242, https://doi.org/10.1016/j.memsci.2011.09.043.
[79] L. Gurreri, A. Filingeri, M. Ciofalo, A. Cipollina, M. Tedesco, A. Tamburini, G. Micale, Electrodialysis with asymmetrically profiled membranes: influence of profiles geometry on desalination performance and limiting current phenomena, Desalination 506 (2021), 115001, https://doi.org/10.1016/j.desal.2021.115001.
[80] R. Kwak, G. Guan, W.K. Peng, J. Han, Microscale electrodialysis: concentration profiling and vortex visualization, Desalination 308 (2013) 138–146, https://doi.org/10.1016/j.desal.2012.07.017.
[81] Y. Tanaka, Principles of ion exchange membrane electrodialysis for saline water desalination, Ion Exch. Technol. I Theory Mater. (2012) 163–209, https://doi.org/10.1007/978-94-007-1700-8_5.